SCIENCE AND TECHNOLOGY OF ADVANCED MATERIALS
2024, VOL. 25, NO. 1, 2404380
https://doi.org/10.1080/14686996.2024.2404380

Effects of the matrix-bounded nanovesicles of high-hydrostatic pressure decellularized tissues on neural regeneration

Mako Kobayashi[a,b], Jun Negishi[b,c], Naoki Ishida[b], Yoshihide Hashimoto[b], Yoshihiro Sasaki[d], Kazunari Akiyoshi[d], Tsuyoshi Kimura[b,e] and Akio Kishida[b]

[a]Department of Materials Processing, Graduate School of Engineering, Tohoku University, Sendai, Miyagi, Japan;
[b]Institute of Biomaterials and Bioengineering, Tokyo Medical and Dental University, Chiyoda, Tokyo, Japan;
[c]Department of Applied Biology, Faculty of Textile Science and Technology, Shinshu University, Ueda City, Nagano, Japan;
[d]Department of Polymer Chemistry, Graduate School of Engineering, Kyoto University, Kyoto, Japan;
[e]Department of Biomedical Engineering, Toyo University, Asaka-city, Saitama, Japan

ABSTRACT

Decellularized tissues have been used as implantable materials for tissue regeneration because of their high biofunctionality. We have reported that high hydrostatic pressured (HHP) decellularized tissue developed in our laboratory exhibits good in vivo performance, but the details of the mechanism are still not known. Based on previous reports of bioactive factors called matrix bound nanovesicles (MBVs) within decellularized tissues, this study aims to investigate whether MBVs are also present in decellularized tissues prepared by HHP decellularization, which is different from the previously reported methods. In this study, we tried to extract bioactive factors from HHP decellularized brain and placenta, and evaluated their effects on nerves in vitro and in vivo, where its effects have been previously reported. The results confirmed that those factors can be extracted even if the decellularization method and tissue of origin differ, and that they have effects on a series of processes toward nerve regeneration, such as neurite outgrowth and nerve fiber repair.

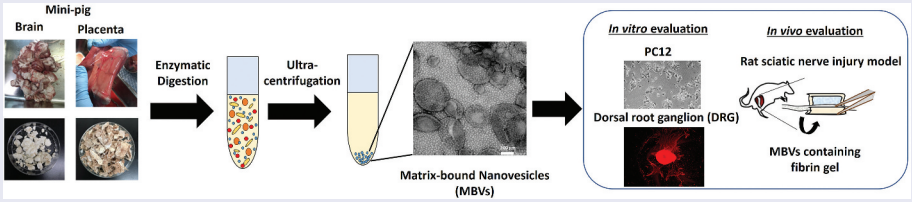

IMPACT STATEMENT

In this study, we evaluated the neuroregenerative effects of matrix-bounded nanovesicles extracted from decellularized tissue using a high hydrostatic pressure method. The results indicate that bioactive factors, including matrix-bounded nanovesicles, can be extracted regardless of the decellularization method and tissue origin.

ARTICLE HISTORY
Received 16 July 2024
Revised 4 September 2024
Accepted 10 September 2024

KEYWORDS
Decellularized tissue; high hydrostatic pressure; extracted components; nerve regeneration

1. Introduction

Decellularized tissue is used as an implantable material for tissue regeneration since it maintains the structure of biological tissue and has high bio-acceptability, growth, and tissue regeneration potential. For example, it is used orthotopically in heart valves and blood vessels [1–6]. In addition, it is applied ectopically in powder or sheet form; in this case, the transplant site is eventually constructed with tissue suitable for the transplant site [7–12]. It is thought that bioactive factors, particularly those within the extracellular matrix (ECM), exert a bioadaptive effect through communication with ectopic tissues and cells. For instance, it is suggested that the constructing remodeling and wound healing have been achieved due to the presence of bioactive peptides [13–15], cytokines and growth factors such as vascular endothelial growth factor (VEGF), basic fibroblast growth factor (bFGF), transforming growth factor (TGF)-β released during decellularized ECM degradation [16–19]. Recently, matrix-bound nanovesicles (MBVs), which are tightly bound to the ECM, have been reported as one of those bioactive factors [20,21]. MBVs are similar to exosomes in terms of particle size and lipid bilayer. However, since they do not express exosome markers, they have been defined as new extracellular vesicles. It has been reported that MBVs can be obtained from a variety of decellularized tissues, but their functions differ

CONTACT Mako Kobayashi mako.kobayashi.e1@tohoku.ac.jp Department of Materials Processing, Graduate School of Engineering, Tohoku University, Aramaki-Aza Aoba, Aoba-Ku, Sendai 6-6-02, Japan

depending on the tissue of origin and preparation method [22,23]. Previously reported bioactive factors were mainly extracted from surfactant decellularized tissues, but these factors derived from high hydrostatic pressure (HHP) decellularized tissue, a physical method without surfactants, have not been characterized. Tissues decellularized with surfactants show no cell adhesion or proliferation *in vitro*, which is thought to be due to residual surfactant. In the presence of surfactants, it is crucial to consider both the stability of the MBV and the toxicity of the surfactant. Consequently, a direct comparison with MBV isolated using the HHP method may not be appropriate. Therefore, in this study, we focused exclusively on MBV isolated by the HHP method to determine whether MBV remains intact after high hydrostatic pressure treatment and to assess its bioactive functions. Therefore, we are attempting to extract those bioactive factors from decellularized tissues prepared by a decellularization method different from existing reports and evaluating its effects on various tissues. Our previous report indicated that bioactive factor containing MBVs can be collected from the small intestine submucosa, urinary bladder matrix, and liver, and that some tissues show bioactive functions in vascular endothelial cells [24]. In this study, we tried to extract bioactive factors from HHP decellularized brain and placenta, and evaluated their effects on nerves in vitro and in vivo, where its effects have been previously reported [25]. First, we attempted to extract bioactive components from the decellularized brain and placenta of miniature swine. The extracted factors are evaluated in vitro for PC12 and mouse dorsal root ganglion elongation. The effect of those factors on nerve in vivo is also examined using the rat sciatic nerve injury model, a commonly used experimental model for studying nerve repair and regeneration. Fibrin gel containing decellularized brain and placenta-derived factor is applied to the site of nerve injury for 6 wk, and the sciatic function index (SFI) of each group of animals is calculated to evaluate functional recovery.

2. Materials and methods

2.1. Materials

Fresh miniature swine brains and placentas were purchased from the Kagoshima Miniature Swine Research Center (Kagoshima, Japan). Magnesium chloride hexahydrate, 0.1 mol/L sodium citrate hydroxide solution, anhydrous ethanol, phosphate-buffered saline (PBS), and Dulbecco's Modified Eagle Medium (DMEM) were obtained from FUJIFILM Wako Pure Chemical Corporation (Osaka, Japan). Rat pheochromocytoma cells (PC12) were purchased from the Japanese Collection of Research Bioresources (Osaka, Japan). Liberase was purchased from Roche Diagnostics (Basel, Switzerland). Mice (C57BL/6JJmsSlc, 7-wk-old) and Sprague-Dawley rats (8-wk-old) were obtained from Sankyo Labo Service Corporation, Inc. (Tokyo, Japan).

2.2. Decellularized tissue preparation

The purchased placentas were immediately placed in saline and washed several times by changing the solution to completely remove blood and clots. Following the identification of the remaining umbilical cord, the thin and transparent amniotic membrane was slowly detached from the placenta. The tissues were then cut into 5-cm-long lengths. Since the brain is a soft and fragile tissue, the brain stem section was lifted using tweezers and removed onto a stainless-steel bat. The thin membrane, that is, the arachnoid matter on the surface, was peeled off and the brain was divided vertically into two sections. The left and right brains were further divided into two sections and cut into approximately 5-cm squares. Trimmed placenta and brain fragments were packed into a plastic bag filled with saline and decellularized under HHP (600 MPa, 30°C for 10 min) (Dr. Chef, Kobelco, Tokyo, Japan). After completion of HHP, the tissues were rinsed with DNase-containing saline at 4°C for 1 wk, 80% ethanol/saline for 3 d, and 0.1 M citrate buffer containing 1% penicillin-streptomycin for 3 d while being shaken.

2.3. Extraction of components from HHP decellularized placenta and brain

The decellularized placenta and brain were then lyophilized (DRC-1100, FDU-2110, EYELA, Tokyo Rikakikai Co., Ltd, Tokyo, Japan) and ground into a powder using electric milling (Tube Mill Control, IKA Japan K, Osaka, Japan). Liberase (0.01 mg/mL) buffer (50 mm Tris (pH 7.5), 5 mm $CaCl_2$, 200 mm NaCl) was added to 10 mg/mL of lyophilized tissue, and the mixture was stirred at 37°C for 24 h. Immediately after solubilization, each solution was centrifuged at 500 × *g*, for 10 min and 10,000 × *g* for 30 min (three times, 4 °C) to remove insoluble collagen fibrils and proteins. The supernatant was collected at each centrifugation step and subjected to an ultracentrifugation step using a Beckman Coulter Optima L-90K Ultracentrifuge (Beckman Coulter, Inc., Brea, CA, U.S.A.) at 100,000 × *g* and 4°C for 70 min. Following the wash process and ultracentrifugation at 100,000 × *g* and 4°C for 30 min, the collected pellets were resuspended in 500 µL of 1×PBS (-) and passed through a 0.22-µm filter (Merck Millipore, Darmstadt, Germany). The final pellets were stored at −20°C until evaluation.

2.4. Characterization of HHP decellularized tissue-derived pellets

TEM was used to observe the morphology and microstructure of MBVs. The ultracentrifuged pellet mixture was loaded onto a carbon-coated copper grid and stained with 2% uranyl acetate to enhance the contrast. The grids were then visualized at 80 kV using a JEM-1400 Flash (Japan Electron Optics Laboratory (JEOL), Tokyo, Japan). A NanoSight LM10 (Malvern Panalytical, Worcestershire, UK) was used to measure the size distribution and concentration of the nanovesicles. The ultracentrifuged pellet solution was diluted with Milli-Q water, and the images were captured five times for 60 s at camera level 13. The particle size and concentration were calculated based on a video analysis.

2.5. RNA isolation and characterization

The total RNA was extracted from the MBVs derived from the decellularized tissues using the miRNeasy Mini Kit with spin columns (QIAGEN, Venlo, The Netherlands) according to the manufacturer's instructions. The isolated RNA was resuspended in RNase/DNase-free water, and the RNA yield was quantified using a NanoDrop 2000 spectrophotometer (Thermo Scientific K, Tokyo, Japan). The quality and size of the RNA were determined through capillary electrophoresis using an RNA 6000 Pico Kit and an Agilent 2100 Bioanalyzer (Agilent Technologies, Santa Clara, CA, U.S.A.) following the manufacturer's protocol.

2.6. Neurite growth assay of PC12

PC12 (4.0×10^3 cells/well) were seeded in a collagen-coated 96-well dish. Following incubation, the MBVs (14 μg/ml) were added to each well, and nerve growth factor (50 ng/ml) was added as a positive control. After 24 h, the cell morphology was observed under a microscope.

2.7. Dorsal root ganglion dissection and plating for culture

This study was approved by the Animal Care and Ethics Committee of Tokyo Medical and Dental University (approval no. A2020-181A). Euthanized mice (C57BL/6JJmsSlc, 7-wk-old) were laid on their faces and shaved with clippers to remove body hair. Their back skins were cut open using scissors to expose the backs. The spines were harvested by inserting a pair of scissors from the waist up to the neck. The vertebrae were then placed in a Petri dish filled with PBS (-) and rinsed gently to remove the blood. The connective tissues surrounding the spines were removed, and the spines were trimmed until white spinal cords were visible. In each case, the vertebral column was held using a tweezer, and the cranial aspect of the spinal cord was pulled from the cranial to the caudal using another tweezer. As the dorsal root ganglions (DRGs) are situated in the intervertebral foramina connected to the spinal cord, they were carefully pulled out of the intervertebral foramen. Following the complete disconnection of the spinal roots and nerves from the DRGs, the isolated DRGs were collected in a Petri dish filled with DMEM.

Subsequently, diluted fibrinogen solution was added to each well. The DRGs were placed in the fibrinogen solution using micro tweezers, one per well. A drop of thrombin solution equal to the volume of the fibrinogen solution was added to the border between the DRG and the fibrinogen solution. The plates were covered with lids and left to stand for 10 min to enable fibrin formation. Next, 0.9 ml of Neurobasal/B-27 solution was gently added to each well. To the negative control wells, 0.1 ml of PBS (-) was added. To the positive control wells, 0.1 ml of brain-derived neurotrophic factor (BDNF) (1 μl of 100 μg/ml BDNF and 99 μl of PBS) was added. The wells to which the samples were added were adjusted with the MBV solution in PBS to obtain the desired concentration (14 μg/ml). 0.1 mL of MBV solution were added to each well. The well plates were incubated in a 5% CO_2 incubator at 37°C for 21 d.

2.8. DRG staining and neurite outgrowth evaluation

The culture plates were removed from the incubator 21 d after the culture was initiated. The medium was removed from each well, and 500 μl of 1×PBS (–) each was added; the wells were gently washed. After two washes with 1×PBS (-), each well was permeabilized with 500 μl of 0.25% Triton X-100 in PBS for 30 min. After washing twice with 1×PBS (-), 500 μl of 5% bovine serum/0.5% Triton X-100 in PBS was added, and the wells were immersed for 90 min for blocking. The primary antibody, β-tubulin (rabbit polyclonal, GTX101279, GeneTex), was diluted 1:500 in 2.5% BSA and 0.5% Triton X-100 in PBS. Thereafter, an antibody diluent was added and left overnight. After washing the solution with 1×PBS (-), it was diluted to a volume of 500 μl by adding 2.5% BSA and 0.5% Triton X-100 in PBS secondary antibody (goat anti-rabbit IgG(H+L) cross-adsorbed secondary antibody, Alexa Fluor 568, Thermo Fisher, 2 μg/ml) and DAPI (10 μg/ml). Following overnight incubation, the cells were washed with 1×PBS (–) and observed under a fluorescence microscope (BZ-X710, Keyence Corp., Osaka, Japan). A hybrid cell count (Keyence, Osaka, Japan) was used to calculate the area of neurite extension in the DRG. The area of the DRG body was subtracted from the combined area of the DRG body and neurite outgrowths to obtain the area of the neurite outgrowth only. These values were substituted into equation (1) to calculate the ratio of the neurite area.

$$\text{Ratio of the neurite outgrowth area}[\%] = \frac{\text{The area of neurite outgrowth}}{\text{The area of DRG body and neurite outgrowth}} \times 100 \quad (1)$$

2.9. Preparation of rat sciatic nerve injury model

This animal study was approved by the Animal Care and Ethics Committee of the Tokyo Medical and Dental University (approval no. A2020-134A). Sprague-Dawley rats (8-wk-old) were anesthetized with isoflurane mixed with oxygen. Under deep anesthesia, the rats were placed in a supine position. In each case, the right hind leg was shaved using a clipper and was placed on a cautery plate covered with wet gauze. The area was wiped and sterilized with iodine and 70% ethanol. The skin of the right thigh was removed using tweezers and dissected using a shear. The sciatic nerve was exposed by incising the muscular layer using surgical shears. After the tissue and membrane surrounding the sciatic nerve were separated, the tip of the monopolar was applied to the sciatic nerve and treated (for 2 s; 6 mm wide). In the untreated group, the muscle layer and skin were sutured with 5–0 Nylon (Monosof, SN-3695). For the other group, fibrin gel containing prepared PBS (-) or decellularized tissue-derived MBVs (14 μg/ml) was applied over the OASIS matrix (Cook Biotech, Inc., Indiana, US) using a two-component syringe. The OASIS matrix with samples containing fibrin gel was placed under the sciatic nerve and wrapped around it. The ends were sutured with 7–0 prolene (Ethicon, 8743 h), and the muscle layer and skin were closed by suturing with 5–0 Nylon.

2.10. Walking track analysis

The sciatic function index (SFI) was measured according to previously described procedures [26]. An acrylic box (30 × 30 × 30) was prepared, in which a rat could move freely, and a video camera was set under the box. The rat was placed in a box and the ceiling was covered with drapes. The rats' walking was recorded on video for 10 min at weekly time points. Five screenshots were taken from the video recording, which clearly showed both the hind limbs and all the toes. The following three points were measured for the uninjured (normal; N) and injured (experimental; E) sides from each image using Fiji (ImageJ open source software): (1) paw length (PL; length between the tip of the center toe and the furthest point of contact on the back of the foot), (2) toe spread (TS; length between the first and fifth digits), and (3) intermediary toe spread (IT; length between the second and fourth digits). The measured values were substituted into the following formula to calculate the SFI [27], and its average value was obtained as follows:

$$\text{SFI} = -38.3 \times \left(\frac{\text{EPL} - \text{NPL}}{\text{NPL}}\right) + 109.5 \times \left(\frac{\text{ETS} - \text{NTS}}{\text{NTS}}\right) + 13.3 \times \left(\frac{\text{EIT} - \text{NIT}}{\text{NIT}}\right) - 8.8 \quad (2)$$

2.11. Luxol fast blue (LFB)/H-E staining of rat sciatic nerve

The combination of LFB staining, which stains the myelin blue, and HE staining, which stains the cytoplasm and nuclei, aids in the detection of myelin sheaths that are difficult to identify through only H-E staining and evaluation of the degree of damage and repair of the sciatic nerve. The dissected rat sciatic nerves were fixed with a neutral-buffered (pH 7.4) solution of 10% formalin in PBS and dehydrated with 70%, 80%, 90%, and 100% ethanol. The samples were then treated with xylene and embedded in paraffin, which was cut into 5-mm-thick sections for staining. The paraffin slices were re-placed in xylene and dehydrated using graded ethanol. Thereafter, they were immersed in distilled water, washed, and replaced in 95% ethanol. After soaking in the LFB staining solution for 24 h (57 °C), the slices were immersed in 95% ethanol. Next, they were washed with distilled water and immersed in a 0.05% lithium carbonate solution for 5 s to obtain a clear stained image. Following immersion in 70% ethanol, the slices were washed gently and immersed in Mayer's hematoxylin solution for 10 min. Following washing with distilled water, the samples were dehydrated using a graded ethanol series.

2.12. Statistical analysis

Figures 3 and 4 are expressed as mean ± standard deviation (SD). The Student's t-test was used to compare the ratio of the neurite area of DRG with the untreated DRG (Figure 3c). The statistical significance was set at $p < 0.05$. Analysis of variance followed by Tukey's multiple comparison test was used to determine statistical significance in the evaluation of the SFI (Figure 4d). The value of $p < 0.05$ was considered significant.

3. Results

To observe the morphology and microstructure of extracted MBVs, the TEM was performed on decellularized miniature swine brains and placenta-derived ultracentrifuged pellets (Figure 1a). Multiple vesicles with lipid membranes were observed in both pellets. Vesicles of various sizes were observed in the brain-derived pellets, ranging from approximately 200 nm to

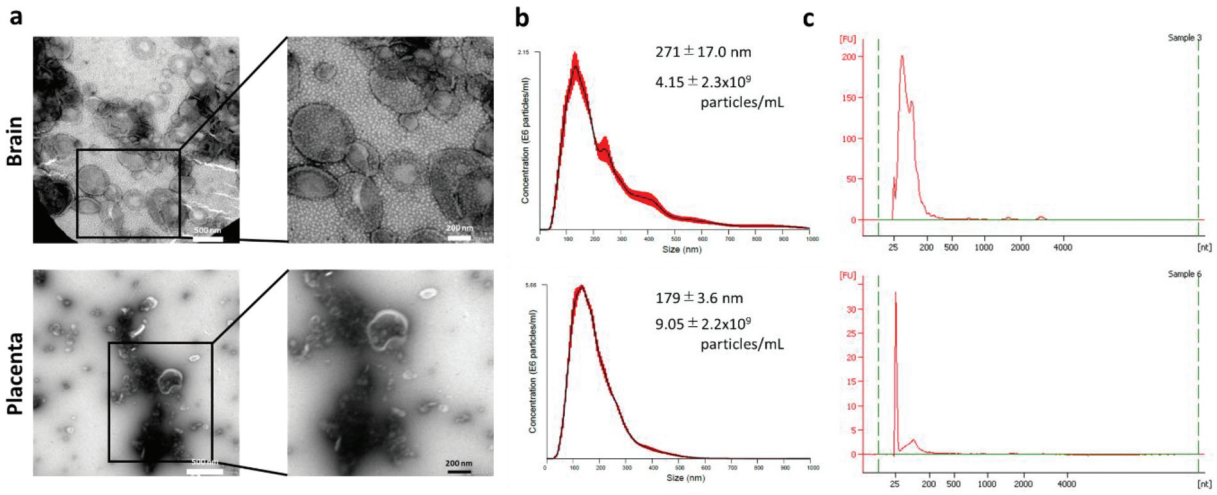

Figure 1. Characterization of decellularized tissue-derived MBVs.

500 nm. Multiple particles of approximately 200 nm in size were identified in the placenta-derived pellet. Figure 1b presents the results of the NTA. In the brain-derived pellets, two peaks were detected at diameters of approximately 200 nm and 400 nm. In contrast, a single peak was detected at a diameter of approximately 150 nm for the placenta-derived pellets. Both the NTA results correlate closely with the TEM images. RNA evaluation indicated peaks of 20–25 nt typical of miRNAs and small RNAs less than 200 nt in length, suggesting that the collected MBVs contained miRNAs and small RNAs (Figure 1c). These results implied MBVs can be extracted from HHP decellularized brain and placenta.

The neuron-like characteristics of differentiated PC12 cells were used to evaluate the neuronal function of extracted components from HHP decellularized tissues. Figure 2c and 2d present images taken 24 h after the addition of pellets from the decellularized brain and placenta, respectively, to PC12. Although not as much as PC12 with NGF added (Figure 2b), neurite extensions were observed in the decellularized derived pellets added cells as compared with the untreated cells (Figure 2a).

The DRGs were harvested from the spinal cord of C57BL/6JJmsSLC mice and embedded in fibrin gel. The nerve growth factor (NGF), decellularized brain, and placenta-derived pellets were added to the medium respectively and cultured for 21 d (Figure 3a). The results of DRG staining with β-tubulin after 21 d of incubation are presented in Figure 3b. All the DRGs survived over the observation period of 21 d. As no neurite outgrowth was observed in the nontreated DRGs and significant neurite outgrowth was observed at NGF- treated DRGs, the results of the sample set as control were properly analyzed. Neurite outgrowth

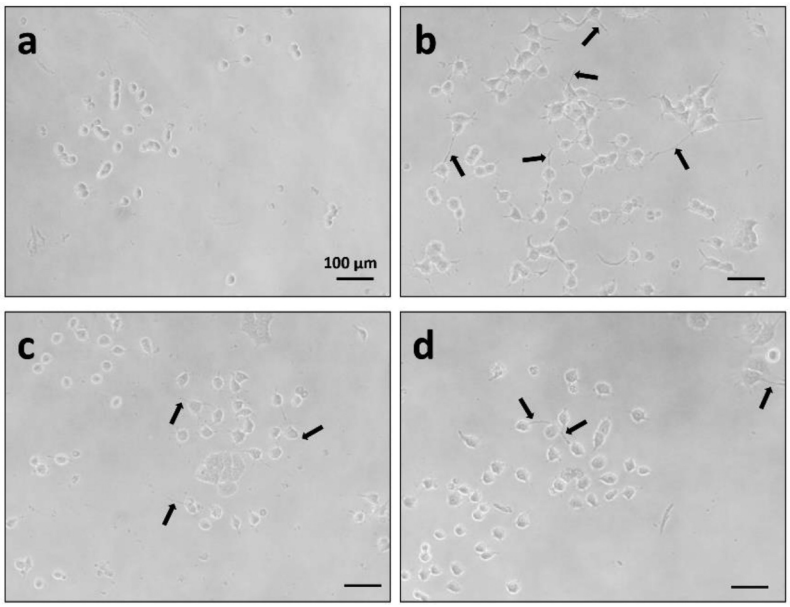

Figure 2. Neurite growth assay of PC12.

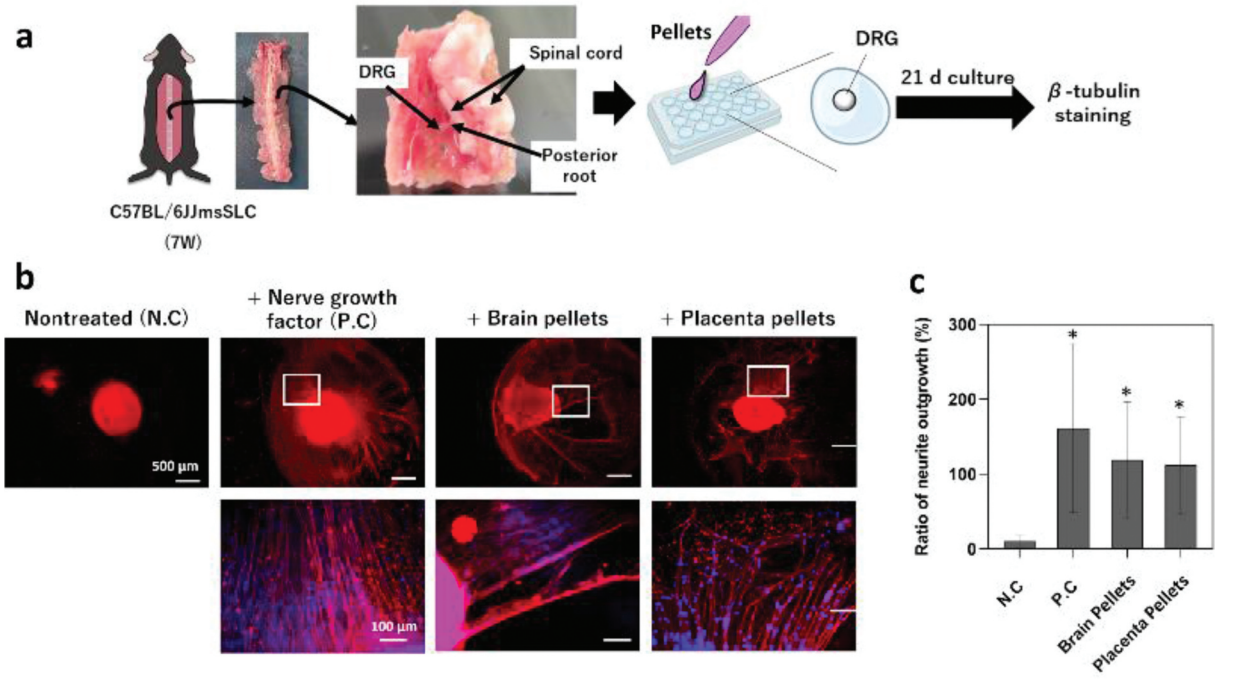

Figure 3. Neurite outgrowth of dorsal root ganglion (DRG) neurons.

was observed in both the decellularized brain and placenta-derived pellets treated DRGs as compared with the nontreated DRGs. A magnified view of the neurite extension from the cell body is presented in Figure 3b. Sharp neurite outgrowths similar to the NGF treated DRGs were observed in the DRGs exposed to the pellets extracted from HHP decellularized brain and placenta. Next, the ratio of the area of neurite outgrowths was determined from the microscopic images obtained using the hybrid cell counter, and calculated by the Equation (1) in the Materials and Methods section. Although the effect beyond the NGF was not confirmed, the addition of the decellularized tissue-derived pellets significantly increased the ratio of the neurite extension area when compared with nontreated (Figure 3c).

A rat sciatic nerve injury model was used to evaluate the effects of the decellularized brain- and placenta-derived pellets on nerve regeneration and functional recovery. On the right side of the lower limb, 6 mm of the sciatic nerve was burnt. A fibrin gel containing decellularized tissue pellets was applied to the OASIS extracellular matrix and wrapped around the nerve injury site (Figure 4a). A walking track analysis was performed every 2 wk. Figure 4b presents screenshots extracted from the video recordings of the walking track analysis for each group. At 2 wk postoperatively, although the rats from the injured group limped, the rats from the other groups walked with curled toes on the damaged side of the paws. By 4 wk postoperatively, all the groups except the injured group walked with their toes slightly extended. At 6 wk, the damaged toes in all the test groups were further widened, indicating nerve recovery. In addition, to assess motor function, the SFI was measured from the video recordings of the animals every 2 wk. The SFI scores were calculated by measuring three parameters for each paw on the normal and experimental sides, as shown in Figure 4c, and substituting them into Equation (2). Figure 4d describes the SFI values for all four groups. The SFI value approaches zero as the recovery trend progresses. No significant difference in recovery was observed between the groups 2 wk after the operation. At 4 wk postoperatively, the injured group had SFI values equivalent to those at 2 wk, whereas the other groups indicated a tendency toward recovery. At 6 wk postoperatively, the SFI values of all the groups were higher, indicating a more advanced recovery. Since the OASIS used for wrapping contained active factors such as growth factors, no significant neurodegenerative effects were observed when comparing fibrin gel alone to gel with MBV added. However, significant nerve regeneration was observed when compared to the damaged group. This suggests that increasing the amount of MBVs added may have a synergistic effect with OASIS. The optimal amount of MBV to be added will be investigated in future studies.

Figure 5 shows the rat sciatic nerve immediately after cauterization and after 6 wk. Adhesion to the surrounding tissue was observed in the injured sciatic nerve. When fibrin gel alone or that containing

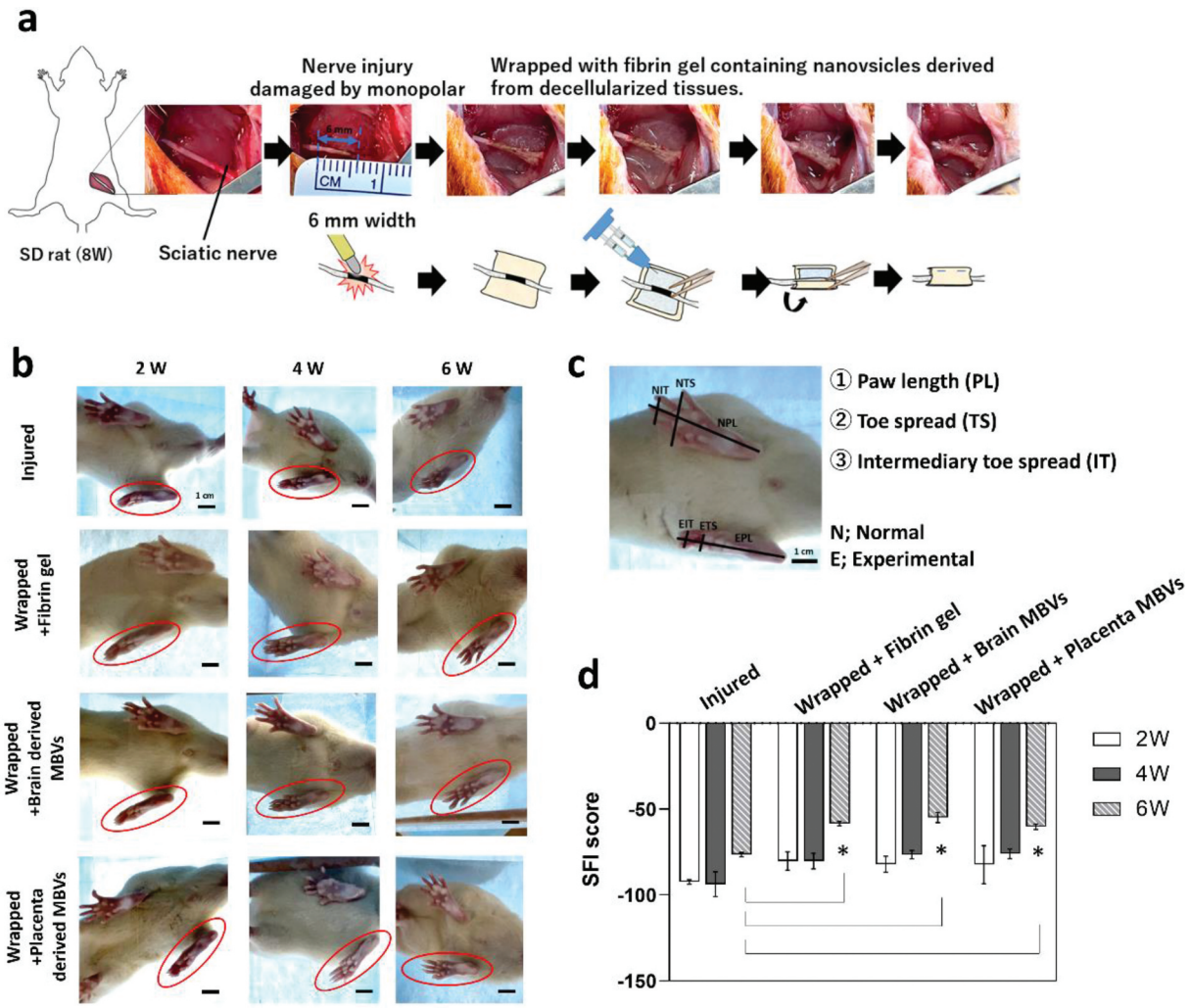

Figure 4. Sciatic nerve injury model and sciatic function index (SFI).

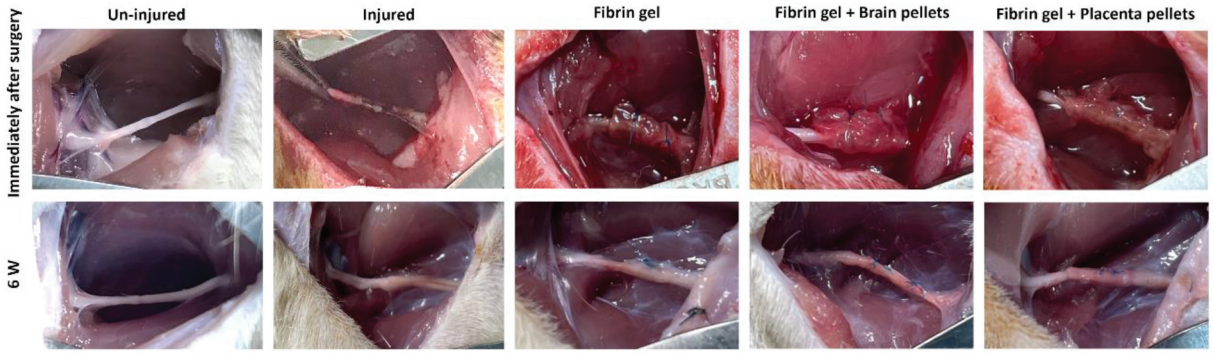

Figure 5. Photographs of sciatic nerves immediately and 6 wk after surgery.

decellularized tissue- derived pellets was applied to the OASIS matrix and wrapped around the sciatic nerve, no adhesion to the surrounding tissue was observed.

Figure 6 presents the results of Luxol fast blue (LFB)/H-E staining 6 wk after cauterization of the rat sciatic nerve. By staining the myelin sheath blue by LFB staining and the cytoplasm and nuclei purple by H-E staining, the degree of sciatic nerve damage and repair is assessed. The un-injured sciatic nerve can be seen to be neatly aligned in the direction of the fibers stained purple. In contrast, the injured sciatic nerve displayed disconnected nerve fibers. In the sciatic nerve of rats to which the decellularized tissue-derived pellets-mixed gel was applied, axons were elongated in the direction of the fibers, similar to the uninjured group.

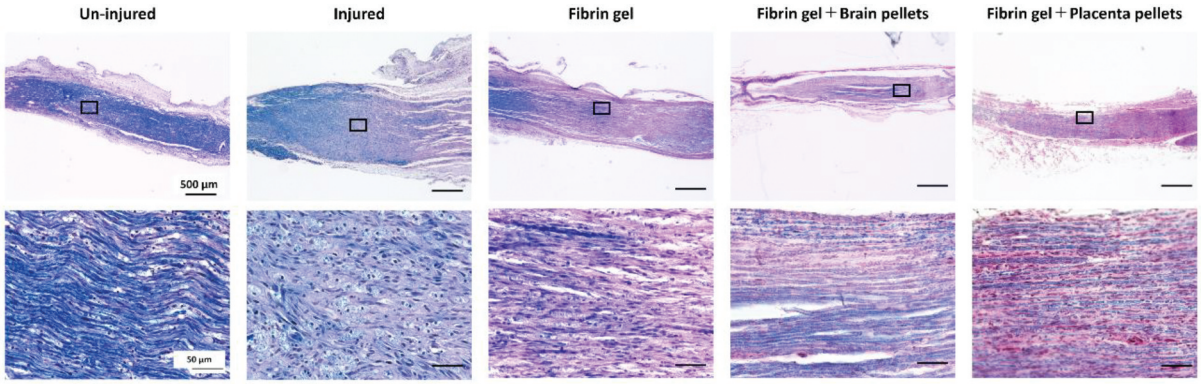

Figure 6. Luxol fast blue/H-E staining of sciatic nerve 6 wk after surgery.

4. Discussion

The surfactant method, a widely used decellularization method, has been reported to be highly functional in vivo [28–30] and products used in clinical practice also use this method [31,32]. HHP treatment, on the other hand, involves immersing biological tissue in a liquid and applying isotropic pressure to disrupt cell membranes, with decellularization completed by a subsequent washing process. The effects of these different decellularization methods on bioactive substances were considered. While the surfactant method dissolves the ECM and may be considered easier to extract bioactive substances in the ECM, there is concern that bioactive factors may leak out during the decellularization process because the ECM structure cannot be maintained due to dissolution and an intense washing process is required to remove surfactant residues. On the other hand, the HHP method has been shown to maintain the ECM structure compared to the surfactant method [6,33], suggesting that MBVs that are strongly bound to the ECM may be retained in an intact state. Therefore, we considered that HHP-decellularized tissue functions in vivo because the bioactive substances maintained in HHP-decellularized tissue are released slowly with ECM degradation over time in vivo. Based on this, the present study investigated whether HHP-decellularized tissue contains the same kinds of bioactive factors as surfactant-decellularized tissue, and analyzed the effects of HHP-decellularized tissue containing bioactive factors on neural regeneration in vitro and in vivo. First, MBV-like vesicles were tried to be extracted from both the decellularized brain and placenta, and evaluated by TEM, NTA, and RNA evaluation. The results of TEM and NTA indicated that vesicles of various sizes, ranging from 100 to 500 nm, were detected in the decellularized brain. In other words, vesicles larger than previously reported were present. The International Society for Extracellular Vesicles (ISEV) defines an extracellular vesicle as 'a particle surrounded by a lipid bilayer without a nucleus (unable to replicate) that is released from a cell' [34]. It is well known that although microvesicles (100–-1,000 nm in diameter), which are a type of extracellular vesicle, have a different production mechanism from exosomes, they share several components and sizes with exosomes, making it difficult to completely separate them [35]. Considering this fact, although MBVs are considered to have different functions from liquid-phase EVs [36], it is possible that MBVs are not only small vesicles such as exosomes but also large vesicles such as microvesicles, similar to the general extracellular secretory granules described by the ISEV. In addition, in RNA evaluation, unlike the placenta-derived MBVs, a large peak was observed at the position of the small RNA of approximately 200 nt in brain-derived MBVs, suggesting that vesicle cargos and functions may differ not only by the tissue of origin but also by vesicle size. Future studies should include a more detailed investigation of the MBV's secretory pathway, cargo, and mechanism of binding to the extracellular matrix.

Furthermore, the collected decellularized brain- and placenta-derived pellets were evaluated *in vitro* by adding them to PC12 and the DRGs. PC12 is derived from rat pheochromocytoma, and it extends neurites and morphologically resembles neurons when stimulated by neurotrophins [37,38]. The DRG is the most frequently used primary cultured neuronal cell and can be used to evaluate the functional properties of peripheral sensory neurons *in vitro* [39]. *In vitro* evaluation using these cells indicated that the addition of decellularized tissue-derived pellets led to neurite outgrowth in the PC12 and DRG. Exosomes derived from mesenchymal stem cells (MSCs) have been

reported to deliver exogenous miRNAs to neurons and promote the neuronal differentiation and recovery of neuronal function [40,41]. Therefore, it is considered that the presence of functional substances such as miRNAs, which affect neurons, in the cargo of vesicles was observed to promote neurite outgrowth and neuronal migration. The specific predicted miRNAs are miR-1 [42], miR-124 [43], miR-133 [44,45], miR-210 [46,47], miRNA 222 [48], miR-340 [49] which are closely related to nerve cell proliferation, migration, and myelination. In the future, it will be necessary to verify the mechanism through which vesicles exert their effects on neurons.

Since the *in vitro* evaluation confirmed the effect of decellularized derived pellets on neurons, as an *in vivo* evaluation, nerve function recovery was observed using a sciatic nerve injury model. Damage to peripheral nerves causes motor paralysis and nerve disorders. The three types of peripheral nerve injuries are as follows: neurapraxia, axonotmesis, and neurotmesis [50]. The lowest degree of nerve injury is called neurapraxia, in which the nerve remains intact but it results in transient weakness. The second degree called axonotmesis, in which the axon is damaged but the surrounding connecting tissue remains intact. The most severe injury is called neurotmesis, in which both the axon and connective tissues are completely disrupted. Surgery for peripheral nerve injury involves compressed tissue or nerve detachment and neurorrhaphy, but after the surgery, the nerves adhere to the surrounding tissues, causing neuropathy such as numbness and pain [51,52]. In addition, it is well known that peripheral nerve regeneration takes time, leading to muscle atrophy and significant muscle weakness [53]. However, nerve induction materials intended for nerve protection and induction do not promote nerve regeneration. Therefore, in this study, a rat sciatic nerve cauterized injury model was prepared to investigate both the prevention of peripheral nerve adhesion to the surrounding tissues and the effect of decellularized tissue-derived pellets on nerve regeneration. We considered that by encapsulating decellularized tissue-derived pellets in fibrin gel and applying it to the damaged peripheral nerves, the nerve-induction-promoting effect of the pellets could be directly applied to the injured area. In addition, the fibrin gel acts as a scaffold material for nerve induction, which is expected to induce nerve regeneration in the early postoperative period, leading to the suppression of muscle atrophy. Although NeuroMend and Axoguard are commercially available nerve wraps [54,55], the fibrin gel containing decellularized tissue derived pellets, an additional bioactive substance applied to the OASIS extracellular matrix in this study, is expected to further accelerate the rate of nerve regeneration. Figure 4 describes that the evaluation of nerve function recovery over a 6-wk period indicates that decellularized tissue-derived pellets have a nerve recovery function. Significant functional recovery was observed in the other study groups when compared with the damage-only study group. However, the effect of decellularized tissue-derived pellets was not significantly different from the SFI values of the study group to which only fibrin gel had been applied. This may simply be attributed to the low content of bioactive factors including growth factors and MBVs. Other reasons include the fact that neurite outgrowth is known to be significantly affected by the complex relationships among several matrix properties such as stiffness [56,57], degradability [58,59], and porosity [60,61]. Thus, by modifying the properties of the hydrogel and wrapping material, it may be possible to create a nerve-wrapping device that induces nerve regenerative recovery and function. In addition, at the 6-wk follow-up, the wrapped nerve exhibited only mild perineural adhesions (Figure 5). This suggests that wrapping the nerve tended to prevent muscle atrophy because nerve damage owing to adhesion with the surrounding tissues was suppressed (data not shown). Although artificial nerves lack environmental factors necessary to induce regenerative axons, such as cytokines, wrapping decellularized tissue-derived pellets-containing gel around the nerve injury site has a nerve regeneration function, and it simultaneously prevents nerve adhesion by wrapping around the nerve.

These results indicate that the effects of HHP decellularized brain- and placenta-derived pellets on neural regeneration were similar, although differences were observed in their characterization. This suggests that the common parts of the brain- and placenta-derived pellets are strongly involved in the mechanism of nerve regeneration. Taken together, it is considered that one of the reasons for the high tissue regenerative potential of HHP decellularized tissue is due to the cooperative manner multi-faceted effects of MBVs.

5. Conclusions

Regardless of decellularization methods, nanosized and membranous vesicles containing miRNA and small RNA can be extracted from HHP-decellularized brain and placenta. The results of *in vitro* and *in vivo* analyses indicate that these decellularized tissue-derived factors affect the comprehensive sequence of events leading to nerve regeneration. This study also provides useful insights into the development of highly functional materials by compositing decellularized tissue-derived factors.

Acknowledgments

We deeply appreciate Mr. Hideki Saga (KM Biologics Co., Ltd) for his generous support and expertise that significantly assisted our research. We acknowledge Dr. Riley Suhar (Genentech, California, US) for helpful discussions and advice

on the experimental design for the dorsal root ganglion dissection, rat sciatic nerve injury model fabrication, and walking track analysis. We acknowledge Yuriko Sakamaki for technical assistance with the TEM observation.

Disclosure statement

No potential conflict of interest was reported by the author(s).

Funding

This work was supported in part by Grants-in-Aid for Scientific Research, KAKENHI [21H04954, 19H04465, 21K20512, 23K17207], the Creative Scientific Research of the Viable Material via Integration of Biology and Engineering from MEXT, and the Cooperative Research Project of the Research Center for Biomedical Engineering from MEXT.

Author contributions

M.K., J.N., N. I., and H.S. performed all the experiments. M. K. and J.N. drafted the manuscript. A.K., Y.H and T.K revised and edited the manuscript. Y.H., Y.S., K.A., and T. K. supervised this study. J.N., H.S., M.K., and A. K. contributed to study conceptualization. All the authors have read and agreed to the published version of the manuscript.

References

[1] Vafaee T, Walker F, Thomas D, et al. Repopulation of decellularised porcine pulmonary valves in the right ventricular outflow tract of sheep: role of macrophages. J Tissue Eng. 2022;13. doi: 10.1177/20417314221102680 PubMed PMID: WOS:000818864600001.

[2] Ramm R, Goecke T, Kohler P, et al. Immunological and functional features of decellularized xenogeneic heart valves after transplantation into GGTA1-KO pigs. Regen Biomater. 2021;8(5). doi: 10.1093/rb/rbab036 PubMed PMID: WOS:000692614600002.

[3] Ramm R, Goecke T, Theodoridis K, et al. Decellularization combined with enzymatic removal of N-linked glycans and residual DNA reduces inflammatory response and improves performance of porcine xenogeneic pulmonary heart valves in an ovine in vivo model. Xenotransplantation. 2020;27(2). doi: 10.1111/xen.12571 PubMed PMID: WOS:000498419100001.

[4] Jenndahl L, Osterberg K, Bogestal Y, et al. Personalized tissue-engineered arteries as vascular graft transplants: a safety study in sheep. Regenerative Ther. 2022;21:331–341. doi: 10.1016/j.reth.2022.08.005 PubMed PMID: WOS:000856709400003.

[5] Kurokawa S, Hashimoto Y, Funamoto S, et al. In vivo recellularization of xenogeneic vascular grafts decellularized with high hydrostatic pressure method in a porcine carotid arterial interpose model. PLOS ONE. 2021;16(7):e0254160. doi: 10.1371/journal.pone.0254160 PubMed PMID: WOS:000678124900009.

[6] Funamoto S, Nam K, Kimura T, et al. The use of high-hydrostatic pressure treatment to decellularize blood vessels. Biomaterials. 2010;31(13):3590–3595. doi: 10.1016/j.biomaterials.2010.01.073 PubMed PMID: WOS:000276254100019.

[7] Xu Y, Yan SH, Chen C, et al. Constructing injectable bone-forming units by loading a subtype of osteoprogenitors on decellularized bone matrix powders for bone regeneration. Front Cell Dev Biol. 2022;10. doi: 10.3389/fcell.2022.910819 PubMed PMID: WOS:000829382400001.

[8] Mesquita FCP, Morrissey J, Lee PF, et al. Cues from human atrial extracellular matrix enrich the atrial differentiation of human induced pluripotent stem cell-derived cardiomyocytes. Biomater Sci. 2021;9(10):3737–3749. doi: 10.1039/d0bm01686a PubMed PMID: WOS:000640800800001.

[9] Tabuchi M, Negishi J, Yamashita A, et al. Effect of decellularized tissue powders on a rat model of acute myocardial infarction. Mater Sciamp; Eng C-Mater For Biol Appl. 2015;56:494–500. doi: 10.1016/j.msec.2015.07.010 PubMed PMID: WOS:000359873900061.

[10] Nasiri B, Yi T, Wu YL, et al. Monocyte recruitment for vascular tissue regeneration. Adv Healthc Mater. 11(22). doi: 10.1002/adhm.202200890 PubMed PMID: WOS:000862070800001.

[11] Brown-Etris M, Milne CT, Hodde JP. An extracellular matrix graft (oasis (R) wound matrix) for treating full-thickness pressure ulcers: a randomized clinical trial. J Tissue Viability. 2019;28(1):21–26. doi: 10.1016/j.jtv.2018.11.001 PubMed PMID: WOS:000461535300004.

[12] Suzuki M, Kimura T, Nakano Y, et al. Preparation of mineralized pericardium by alternative soaking for soft–hard interregional tissue application. J Biomed Mater Res. 2023;111(2):198–208. doi: 10.1002/jbm.a.37445 PubMed PMID: WOS:000850497300001.

[13] Agrawal V, Tottey S, Johnson SA, et al. Recruitment of progenitor cells by an extracellular matrix cryptic peptide in a mouse model of digit amputation. Tissue Eng Part A. 2011;17(19–20):2435–2443. doi: 10.1089/ten.tea.2011.0036 PubMed PMID: WOS:000295155800007.

[14] Maquart F, Bellon G, Pasco S, et al. Matrikines in the regulation of extracellular matrix degradation. Biochimie. 2005;87(3–4):353–360. doi: 10.1016/j.biochi.2004.10.006 PubMed PMID: WOS:000228156900013.

[15] Davis GE, Bayless KJ, Davis MJ, et al. Regulation of tissue injury responses by the exposure of matricryptic sites within extracellular matrix molecules. Am J Pathol. 2000;156(5):1489–1498. doi: 10.1016/s0002-9440(10)65020-1 PubMed PMID: WOS:000086970300003.

[16] Hodde JP, Record RD, Liang HA, et al. Vascular endothelial growth factor in porcine-derived extracellular matrix. Endothelium-New Y. 2001;8(1):11–24. doi: 10.3109/10623320109063154 PubMed PMID: WOS:000168451500002.

[17] VoytikHarbin SL, Brightman AO, Kraine MR, et al. Identification of extractable growth factors from small intestinal submucosa. J Cell Biochem. 1997;67(4):478–491. doi: 10.1002/(sici)1097-4644(19971215)67:4<478:aid-jcb6>3.0.co;2-p PubMed PMID: WOS:A1997YE69900006.

[18] Vorotnikova E, McIntosh D, Dewilde A, et al. Extracellular matrix-derived products modulate

endothelial and progenitor cell migration and proliferation in vitro and stimulate regenerative healing in vivo. Matrix Biol. 2010;29(8):690–700. doi: 10.1016/j.matbio.2010.08.007 PubMed PMID: WOS:000285698600006.

[19] Reing JE, Zhang L, Myers-Irvin J, et al. Degradation products of extracellular matrix affect cell migration and proliferation. Tissue Eng Part A. 2009;15(3):605–614. doi: 10.1089/ten.tea.2007.0425 PubMed PMID: WOS:000263913900016.

[20] Huleihel L, Hussey GS, Naranjo JD, et al. Matrix-bound nanovesicles within ECM bioscaffolds. Sci Adv. 2016;2(6). doi: 10.1126/sciadv.1600502 PubMed PMID: WOS:000380073800034.

[21] Gshldclgbbrtf B, Dziki JL, Lee YC. Matrix bound nanovesicle-associated IL-33 activates a pro-remodeling macrophage phenotype via a non-canonical, ST2-independent pathway. 2019 Mar:26–35. doi: 10.1016/j.regen.2019.01.001

[22] Turner NJ, Quijano LM, Hussey GS, et al. Matrix bound nanovesicles have tissue-specific characteristics that suggest a regulatory role. Tissue Eng Part A. 2022;28(21–22):879–892. doi: 10.1089/ten.tea.2022.0091 PubMed PMID: WOS:000892069000001.

[23] Quijano LM, Naranjo JD, El-Mossier SO, et al. Matrix-Bound Nanovesicles: the effects of isolation method upon yield, purity, and function. Tissue Eng Part C-Methods. 2020;26(10):528–540. doi: 10.1089/ten.tec.2020.0243 PubMed PMID: WOS:000581816900003.

[24] Mako Kobayashi NI, Hashimoto Y, Negishi J, et al. Extraction and biological evaluation of matrix-bound nanovesicles (MBVs) from high-hydrostatic pressure-decellularized tissues. Int J Mol Sci. 2022;23(16):8868. doi: 10.3390/ijms23168868

[25] van der Merwe Y, Faust AE, Sakalli ET, et al. Matrix-bound nanovesicles prevent ischemia-induced retinal ganglion cell axon degeneration and death and preserve visual function. Sci Rep. 2019;9. doi: 10.1038/s41598-019-39861-4 PubMed PMID: WOS:000460381600055.

[26] Suhar RA, Marquardt LM, Song S, et al. Elastin-like proteins to support peripheral nerve regeneration in guidance conduits. ACS Biomater Sciamp; Eng. 2021;7(9):4209–4220. doi: 10.1021/acsbiomaterials.0c01053 PubMed PMID: WOS:000696370300008.

[27] Bain JR, Mackinnon SE, Hunter DA. Functional-evaluation of complete sciatic, peroneal, and posterior tibial nerve lesions in the rat. Plast Reconstr Surg. 1989;83(1):129–136. doi: 10.1097/00006534-198901000-00024 PubMed PMID: WOS:A1989R673200024.

[28] Vafaee T, Thomas D, Desai A, et al. Decellularization of human donor aortic and pulmonary valved conduits using low concentration sodium dodecyl sulfate. J Tissue Eng Regen Med. 2018;12(2):E841–E53. doi: 10.1002/term.2391 PubMed PMID: WOS:000425184900018.

[29] Wilcox HE, Korossis SA, Booth C, et al. Biocompatibility and recellularization potential of an acellular porcine heart valve matrix. J Heart Valve Dis. 2005;14(2):228–237. PubMed PMID: WOS:000227579700014.

[30] da Costa Fda, Costa A, Prestes R, et al. The early and midterm function of decellularized aortic valve allografts. Ann Thorac Surg. 2010;90(6):1854–1861. doi: 10.1016/j.athoracsur.2010.08.022 PubMed PMID: WOS:000284463200025.

[31] Sarikouch S, Horke A, Tudorache I, et al. Decellularized fresh homografts for pulmonary valve replacement: a decade of clinical experience. Eur J Cardio-Thorac Surg. 2016;50(2):281–290. doi: 10.1093/ejcts/ezw050 PubMed PMID: WOS:000383206100020.

[32] Sarikouch S, Theodoridis K, Hilfiker A, et al. Early insight into in vivo recellularization of cell-free allogenic heart valves. Ann Thorac Surg. 2019;108(2):581–589. doi: 10.1016/j.athoracsur.2019.02.058 PubMed PMID: WOS:000476514900061.

[33] Hashimoto Y, Hattori S, Sasaki S, et al. Ultrastructural analysis of the decellularized cornea after interlamellar keratoplasty and microkeratome-assisted anterior lamellar keratoplasty in a rabbit model. Sci Rep. 2016;6. doi: 10.1038/srep27734 PubMed PMID: WOS:000377671500001.

[34] Thery C, Witwer KW, Aikawa E, et al. Minimal information for studies of extracellular vesicles 2018 (MISEV2018): a position statement of the international society for extracellular vesicles and update of the MISEV2014 guidelines. J Extracell Vesicles. 2018;7(1). doi: 10.1080/20013078.2018.1535750 PubMed PMID: WOS:000452068900001.

[35] Raposo G, Stoorvogel W. Extracellular vesicles: exosomes, microvesicles, and friends. J Cell Biol. 2013;200(4):373–383. doi: 10.1083/jcb.201211138 PubMed PMID: WOS:000315157600002.

[36] Hussey GS, Molina CP, Cramer MC, et al. Lipidomics and RNA sequencing reveal a novel subpopulation of nanovesicle within extracellular matrix biomaterials. Sci Adv. 2020;6(12). doi: 10.1126/sciadv.aay4361 PubMed PMID: WOS:000521937000015.

[37] Vaudry D, Stork PJS, Lazarovici P, et al. Signaling pathways for PC12 cell differentiation: making the right connections. Science. 2002;296(5573):1648–1649. doi: 10.1126/science.1071552 PubMed PMID: WOS:000175976200044.

[38] Das KP, Freudenrich TM, Mundy WR. Assessment of PC12 cell differentiation and neurite growth: a comparison of morphological and neurochemical measures. Neurotoxicol Teratol. 2004;26(3):397–406. doi: 10.1016/j.ntt.2004.02.006 PubMed PMID: WOS:000221366500006.

[39] Caroline Perner CLS. Protocol for dissection and culture of murine dorsal root ganglia neurons to study neuropeptide release. STAR Protocols,; 2021. p. 100333. doi: 10.1016/j.xpro.2021.100333 PMCID: PMC7876630.

[40] Yu B, Zhang XM, Li XR. Exosomes derived from mesenchymal stem cells. Int J Mol Sci. 2014;15(3):4142–4157. doi: 10.3390/ijms15034142 PubMed PMID: WOS:000334444700047.

[41] Yin K, Wang SH, Zhao RC. Exosomes from mesenchymal stem/stromal cells: a new therapeutic paradigm. Biomark Res. 2019;7. doi: 10.1186/s40364-019-0159-x PubMed PMID: WOS:000463731700001.

[42] Yi S, Yuan Y, Chen QQ, et al. Regulation of Schwann cell proliferation and migration by miR-1 targeting brain-derived neurotrophic factor after peripheral nerve injury. Sci Rep. 2016;6. doi: 10.1038/srep29121 PubMed PMID: WOS:000379180400001.

[43] Yang YX, Ye YQ, Kong CG, et al. MiR-124 enriched exosomes promoted the M2 polarization of microglia and enhanced hippocampus neurogenesis after traumatic brain injury by inhibiting TLR4 pathway.

Neurochem Res. 2019;44(4):811–828. doi: 10.1007/s11064-018-02714-z PubMed PMID: WOS:000462990500007.

[44] Xin HQ, Li Y, Liu ZW, et al. MiR-133b promotes neural plasticity and functional recovery after treatment of stroke with multipotent mesenchymal stromal cells in rats via transfer of exosome-enriched extracellular particles. Stem Cells. 2013;31(12):2737–2746. doi: 10.1002/stem.1409 PubMed PMID: WOS:000327736000014.

[45] Klimovich P, Rubina K, Sysoeva V, et al. New frontiers in peripheral nerve regeneration: concerns and remedies. Int J Mol Sci. 2021;22(24). doi: 10.3390/ijms222413380 PubMed PMID: WOS:000738072300001.

[46] Li RF, Bao LZ, Hu W, et al. Expression of miR-210 mediated by adeno-associated virus performed neuroprotective effects on a rat model of acute spinal cord injury. Tissue & Cell. 2019;57:22–33. doi: 10.1016/j.tice.2019.02.004 PubMed PMID: WOS:000462932200004.

[47] Tang X, Sun C. The roles of MicroRNAs in neural regenerative medicine. Exp Neurol. 2020;332. doi: 10.1016/j.expneurol.2020.113394 PubMed PMID: WOS:000556334300011.

[48] Zhao H, Yao RR, Cao XD, et al. Neuroimmune modulation following traumatic stress in rats: evidence for an immunoregulatory cascade mediated by c-Src, miRNA222 and PAK1. J Neuroinflammation. 2011;8(1):159. doi: 10.1186/1742-2094-8-159 PubMed PMID: WOS:000299055900001.

[49] Qing LM, Chen HW, Tang JY, et al. Exosomes and their MicroRNA cargo: new players in peripheral nerve regeneration. Neurorehabil Neural Repair. 2018;32(9):765–776. doi: 10.1177/1545968318798955 PubMed PMID: WOS:000444981100003.

[50] Tapadia M, Mozaffar T, Gupta R. Compressive neuropathies of the upper extremity: update on pathophysiology, classification, and electrodiagnostic findings. J Hand Surg-Am Volume. 2010;35A(4):668–677. doi: 10.1016/j.jhsa.2010.01.007 PubMed PMID: WOS:000276604600026.

[51] Griffin MF, Malahias M, Hindocha S, et al. Peripheral nerve injury: principles for repair and regeneration. Open Orthop J; 2014. p. 199–203. doi:10.2174/1874325001408010199 PMCID: PMC4110386.

[52] Staff NP, Engelstad J, Klein CJ, et al. Post-surgical inflammatory neuropathy. Brain. 2010;133:2866–2880. doi: 10.1093/brain/awq252 PubMed PMID: WOS:000282423100005.

[53] Gordon T. Peripheral nerve regeneration and muscle reinnervation. Int J Mol Sci. 2020;21(22). doi: 10.3390/ijms21228652 PubMed PMID: WOS:000594932800001.

[54] Aigner TB, Haynl C, Salehi S, et al. Nerve guidance conduit design based on self-rolling tubes. Mater Today Bio. 2020;5. doi: 10.1016/j.mtbio.2020.100042 PubMed PMID: WOS:000546331600007.

[55] Suryavanshi JR, Cox C, Osemwengie BO, et al. Sutureless repair of a partially transected median nerve using tisseel glue and axoguard nerve protector: a case report. Microsurgery. 2020;40(8):896–900. doi: 10.1002/micr.30593 PubMed PMID: WOS:000528340100001.

[56] Man AJ, Davis HE, Itoh A, et al. Neurite outgrowth in fibrin gels is regulated by substrate stiffness. Tissue Eng Part A. 2011;17(23–24):2931–2942. doi: 10.1089/ten.tea.2011.0030 PubMed PMID: WOS:000298077900005.

[57] Zhou WD, Blewitt M, Hobgood A, et al. Comparison of neurite growth in three dimensional natural and synthetic hydrogels. J Biomater Sci-Polym Ed. 2013;24(3):301–314. doi: 10.1080/09205063.2012.690277 PubMed PMID: WOS:000316011600005.

[58] Sarker MD, Naghieh S, McInnes AD, et al. Bio-fabrication of peptide-modified alginate scaffolds: printability, mechanical stability and neurite outgrowth assessments. Bioprinting. 2019;14:e00045. doi: 10.1016/j.bprint.2019.e00045

[59] Mahoney MJ, Anseth KS. Three-dimensional growth and function of neural tissue in degradable polyethylene glycol hydrogels. Biomaterials. 2006;27(10):2265–2274. doi: 10.1016/j.biomaterials.2005.11.007 PubMed PMID: WOS:000235389700011.

[60] Thomas AM, Kubilius MB, Holland SJ, et al. Channel density and porosity of degradable bridging scaffolds on axon growth after spinal injury. Biomaterials. 2013;34(9):2213–2220. doi: 10.1016/j.biomaterials.2012.12.002 PubMed PMID: WOS:000315179200007.

[61] Sudhin Thampi AT, Muthuvijayan V, Parameswaran R. Accelerated outgrowth of neurites on graphene oxide-based hybrid electrospun fibro-porous polymeric substrates. ACS Appl Bio Mater. 2020;3(4):2160–2169. doi: 10.1021/acsabm.0c00026